

Nonstabilizerness in Stark many-body localization

Han-Ze Li,^{1,2} Yi-Rui Zhang,¹ Yu-Jun Zhao,^{1,3} Xuyang Huang,¹ and Jian-Xin Zhong^{1,3,*}

¹*Institute for Quantum Science and Technology, Shanghai University, Shanghai 200444, China*

²*Department of Physics, National University of Singapore, Singapore 117542, Singapore*

³*School of Physics and Optoelectronics, Xiangtan University, Xiangtan 411105, China*

Quantum many-body disorder-free localization can suppress transport while still allowing the buildup of computationally costly non-Clifford resources. In a transverse-field Ising chain realizing disorder-free Stark many-body localization, we show that the stabilizer Rényi entropy remains nonzero and grows slowly to a finite plateau deep in the strong Stark-field regime, with strong initial-state selectivity. As the Stark field strength increases, long-time magic and entanglement consistently signal a crossover from ergodic to constrained localized dynamics. These results establish nonstabilizerness (“magic”) as a practical complexity probe for disorder-free ergodicity breaking and constrained localization, with direct relevance to benchmarking and designing near-term quantum simulators, and fill a gap in the understanding of nonstabilizerness in disorder-free many-body localization.

I. INTRODUCTION

The quest to identify the distinct quantum resources that enable computational advantage over classical devices lies at the heart of modern quantum information science [1–8]. While multipartite entanglement is a necessary condition for quantum speedup, it is not sufficient; according to the Gottesman-Knill theorem [9, 10] states generated by Clifford circuits can be highly entangled yet efficiently simulated on classical computers in polynomial time. To capture the true cost of quantum simulation and the potential for universality, one must quantify *nonstabilizerness* or *magic* [11–63]—the resource required to implement non-Clifford gates or to prepare states outside the stabilizer manifold. Recent advances have established nonstabilizerness not merely as a static resource for fault-tolerant computing [64–67], but as a dynamical probe for many-body physics, intimately linked to quantum chaos [68–79], information scrambling [71, 79–88], and the emergence of unitary t -designs [89–97]. Understanding how this costly resource evolves under Hamiltonian dynamics is therefore crucial for characterizing the inherent computational complexity of quantum matter.

In parallel, the study of ergodicity breaking and the breakdown of thermalization in isolated quantum systems has identified many-body localization (MBL) as one particularly robust mechanism [98–106]. While initial wisdom focused on disorder-driven systems [98], it has become evident that disorder is not a prerequisite for localization; robust ergodicity breaking can also emerge in disorder-free systems governed by strong kinetic constraints [107–111]. A prime example is *Stark Many-Body Localization* (SMBL), which arises in interacting lattice models subject to a strong linear potential gradient [112]. In this regime, the conservation of energy imposes severe constraints on particle hopping—processes that change the center of mass are resonantly suppressed—leading to a mechanism rooted in the Wannier-Stark ladder [109, 113–118]. In the limit of a strong tilt, these constraints can induce a phenomenon akin to Hilbert space fragmentation [119],

where the accessible Hilbert space shatters into exponentially many disconnected dynamical sectors, effectively arresting transport [107–109, 120]. This connection places SMBL at the intersection of localization, constrained dynamics, and the emergence of non-thermal phases in clean quantum matter [107, 108, 112].

The behavior of nonstabilizerness in these non-ergodic regimes presents a fundamental theoretical puzzle. In ergodic systems, magic grows rapidly, driven by the scrambling of information into complex Pauli strings [13, 121], eventually saturating to values typical of the Haar measure [12, 122]. Conversely, in MBL systems, the dynamics are restricted to a small submanifold [98, 123]. Pioneering studies have recently begun to chart this complexity frontier in *disordered* MBL systems [124, 125], suggesting that nonstabilizerness can serve as a sharp order parameter for the transition. However, interpreting these findings is complicated by the inherent heterogeneity of disordered landscapes: rare Griffiths singularities and thermal inclusions can dominate long-time dynamics [126–128], obscuring the intrinsic properties of the localized phase. More fundamentally, the localization mechanism in Stark systems—arising from kinetic constraints and fragmentation rather than randomness [109, 112, 129]—imposes a distinct dynamical structure. A fundamental tension therefore emerges: Does the shattering of the Hilbert space in SMBL impose a hard bound on nonstabilizerness, effectively Cliffordizing the dynamics? Or does the system find higher-order resonant pathways [109, 130] to generate magic, revealing a rich dynamical structure hidden beneath the frozen density profile?

In this paper, we study the dynamical generation of nonstabilizerness in a clean constrained system exhibiting Stark many-body localization. Focusing on the tilted transverse-field Ising chain in Eq. (1), we quantify complexity using the stabilizer Rényi entropy (SRE) $M_2(t)$ and compare it with bipartite entanglement growth for several global-quench protocols starting from representative product states. Our analysis reveals that, deep in the strong-tilt regime, nonstabilizerness still grows over extended time windows before saturating, but the growth is strongly slowed and becomes highly initial-state dependent. Long-time observables show a clear ETH-SMBL crossover: $\Delta M_2 \equiv M_2^{\text{Haar}} - M_2$ increases sharply

* jxzhong@shu.edu.cn

with the tilt. It exhibits consistent finite-size crossing behavior, in parallel with the suppression of half-chain entanglement. In the strong-tilt limit, we further derive an effective diagonal description via a Schrieffer-Wolff expansion, where emergent diagonal couplings are factorially suppressed with distance along the Wannier-Stark ladder, providing a natural explanation for the slow magic growth. We also outline a trapped-ion digital-simulation protocol in which both $M_2(t)$ and Rényi-2 entanglement can be extracted from the same local randomized-measurement data. Our work opens a new route to using nonstabilizerness as a quantitative probe of constrained localization and fragmentation, bridging quantum-information complexity with disorder-free ergodicity breaking.

The remainder of this paper is organized as follows. Section II introduces the model and diagnostics. Section III presents the strong-tilt analytical theory. Section IV reports numerical results for the dynamics and scaling of $M_2(t)$ and its relation to entanglement, including the ETH-SMBL crossover analysis. Section V discusses an experimental implementation, and Sec. VI concludes.

II. MODEL AND DIAGNOSTICS

A. Model

We consider a one-dimensional chain of L qubits with open boundary conditions. On site i , the Pauli operators are denoted by X_i, Y_i, Z_i and I_i the identity. The dynamics are governed by a transverse-field Ising Hamiltonian subject to a purely linear potential gradient,

$$H = J \sum_{i=0}^{L-1} Z_i Z_{i+1} h \sum_{i=0}^L X_i + F \sum_{i=0}^L i Z_i. \quad (1)$$

Here J is the Ising coupling, h is the transverse-field strength, and F is the Stark gradient, which induces a site-dependent longitudinal field increasing linearly along the chain. Open boundary conditions are adopted since the linear tilt explicitly breaks translation invariance.

B. Diagnostics

We characterize the dynamics using two complementary diagnostics. Bipartite entanglement quantifies quantum correlations across a spatial cut, while the stabilizer Rényi entropy *SRE* directly probes nonstabilizerness, namely how far the evolving state lies outside the stabilizer manifold and therefore beyond efficient Clifford simulation.

Firstly, for a pure state $|\Psi\rangle$ of the full chain and a subsystem R with complement R^c , the reduced density matrix is $\rho_R := \text{Tr}_{R^c}(|\Psi\rangle\langle\Psi|)$. The Rényi entanglement entropy [131, 132] of order α is $S_\alpha(\rho_R) := \frac{1}{1-\alpha} \log \text{Tr}(\rho_R^\alpha)$ for $\alpha \in (0, 1) \cup (1, \infty)$, and it probes the full eigenvalue spectrum of ρ_R , with larger α emphasizing the largest eigenvalues more strongly. The von

Neumann entropy is obtained in the limit $\alpha \rightarrow 1$ and is given by

$$S_1(\rho_R) := -\text{Tr}(\rho_R \log \rho_R). \quad (2)$$

In the main text we focus on the half-chain bipartition $|R| = L/2$ and report $S_{L/2}$ as a standard indicator distinguishing ergodic from constrained dynamics.

On the other side, entanglement alone does not fully capture computational complexity, since stabilizer states can be highly entangled yet remain classically efficiently simulable. To directly diagnose nonstabilizerness we employ the SRE [13, 14]. Let $\mathcal{P}_L := \{I, X, Y, Z\}^{\otimes L}$ denote the set of L -qubit Pauli strings up to overall phases, and let $D := 2^L$ be the Hilbert-space dimension. For a pure state $|\Psi\rangle$ we define the stabilizer purity $P_\alpha(\Psi) := \frac{1}{D} \sum_{P \in \mathcal{P}_L} |\langle\Psi|P|\Psi\rangle|^{2\alpha}$, and the SRE

$$M_\alpha(\Psi) := \frac{1}{1-\alpha} \log_2 P_\alpha(\Psi), \quad \alpha > 0, \alpha \neq 1, \quad (3)$$

with M_1 defined by the limit $\alpha \rightarrow 1$. Throughout we fix $\alpha = 2$ and denote $M_2 \equiv M_{\alpha=2}$. With this convention one has $M_2 \geq 0$, and $M_2 = 0$ holds if and only if $|\Psi\rangle$ is a pure stabilizer state. Moreover, M_2 is invariant under Clifford unitaries, since Cliffords permute Pauli strings under conjugation and thus preserve the multiset of Pauli moments, and it is additive under tensor products, $M_2(\Psi \otimes \Phi) = M_2(\Psi) + M_2(\Phi)$. Consequently, any increase of M_2 under unitary time evolution witnesses the generation of non-Clifford resources. More importantly, SRE is an experimental observable [133–135].

As a reference for highly complex states we compare M_2 to its Haar-random value [13, 17, 18, 122]. For an L -qubit Hilbert space of dimension $D = 2^L$, the expected SRE-2 of Haar-random pure states is

$$M_2^{\text{Haar}} = \log_2(2^L + 3) - 2, \quad (4)$$

which approaches $L - 2$ at large L . Reaching this benchmark is, however, a dynamical question whose answer depends on the structure of the unitary evolution. In random unitary circuits [16–18, 25, 36], local randomness is injected layer by layer and M_2 typically approaches M_2^{Haar} at depths that grow only slowly with L [122], often logarithmically or polylogarithmically. Generic Floquet dynamics without conservation laws can display similarly fast, circuit-like scrambling [90–92]. In contrast, for local Hamiltonian evolution the approach to the Haar benchmark is constrained by locality, since operator support and information must propagate across the chain, leading to an approach time that grows at least linearly with L , while the accessible-time saturation may remain below M_2^{Haar} due to residual structure from locality, symmetries, and conserved quantities. These considerations are particularly relevant for the setup studied here, where the linear potential further restricts resonant processes and can strongly suppress the generation of magic. For convenience we will also use the deviation from the Haar benchmark [34], $\Delta M_2 := M_2^{\text{Haar}} - M_2$, so that ergodic dynamics correspond to small ΔM_2 , while constrained or nonergodic regimes exhibit a parametrically larger deviation.

We investigate global quenches governed by $|\Psi(t)\rangle = e^{-iHt}|\Psi_0\rangle$ using four families of initial product states: (i) a specific computational-basis state $|z_\star\rangle$ chosen to minimize the diagonal energy $|\langle z|H_{\text{diag}}|z\rangle|$; (ii) the fully polarized states along the transverse axes, $|\Psi_X\rangle = |+\rangle^{\otimes L}$ with $|+\rangle = \frac{1}{\sqrt{2}}(|0\rangle + |1\rangle)$ and $|\Psi_Y\rangle = |+_y\rangle^{\otimes L}$ with $|+_y\rangle = \frac{1}{\sqrt{2}}(|0\rangle + i|1\rangle)$; and (iii) an ensemble of Haar-random product states, over which we average the observables.

III. ANALYTICAL RESULTS

To capture the magic dynamics in the strong-tilt regime, we derive an effective diagonal Hamiltonian by integrating out the off-resonant transverse-field processes. In the strong-tilt limit $F \gg J, h$, we consider Eq. (1) as

$$H = H_0 + V, \quad (5)$$

with $H_0 = \sum_j (Fj Z_j + JZ_j Z_{j+1})$ and $V = h \sum_j X_j$, where X_j and Z_j are Pauli operators on site j . We perform a Schrieffer-Wolff transformation $H_{\text{eff}} = e^S H e^{-S}$ with $S^\dagger = -S$, choosing $[H_0, S^{(1)}] = V$ to eliminate the leading off-diagonal processes. Truncating consistently yields $H_{\text{eff}} = H_0 + \frac{1}{2}[S^{(1)}, V] + O(h^3)$, and higher SW orders generate diagonal multi-spin Z -string couplings. We retain only the diagonal sector $H_{\text{eff}}^{(d)}$ and define $J_{\text{eff}}(r)$ as the typical strength of diagonal two-body couplings at separation r (Cf. Appendix A for the more details). In the strong-tilt regime, energy denominators accumulate along the Stark ladder, leading to a factorial suppression

$$J_{\text{eff}}(r) \sim J_0 \frac{(h/F)^{r-1}}{(r-1)!}, \quad (6)$$

with $J_0 \sim h$. In the dephasing-dominated regime $tJ_0 \gtrsim 1$, the dephasing front $r(t)$ follows from $tJ_{\text{eff}}(r(t)) \sim 1$ and can be written in closed form as

$$r(t) \simeq 1 + \frac{\ln(tJ_0)}{W_0\left(\frac{\ln(tJ_0)}{e h/F}\right)}, \quad (7)$$

where W_0 is the principal branch of the Lambert W function defined by $W_0(x)e^{W_0(x)} = x$. We then use a saturating closure for the SRE-2 observable,

$$M_2(t) \simeq M_{\text{sat}} \tanh(\gamma r(t)), \quad (8)$$

with M_{sat} the finite-size plateau and γ a growth coefficient. Full derivations are provided in Appendix A.

IV. NUMERICAL RESULTS

This section examines how the Stark gradient F shapes the growth and saturation of nonstabilizerness $M_2(t)$, its dependence on the initial state and system size L , and its relation to entanglement dynamics. As a reference for complete randomization we use the Haar benchmark M_2^{Haar} ,

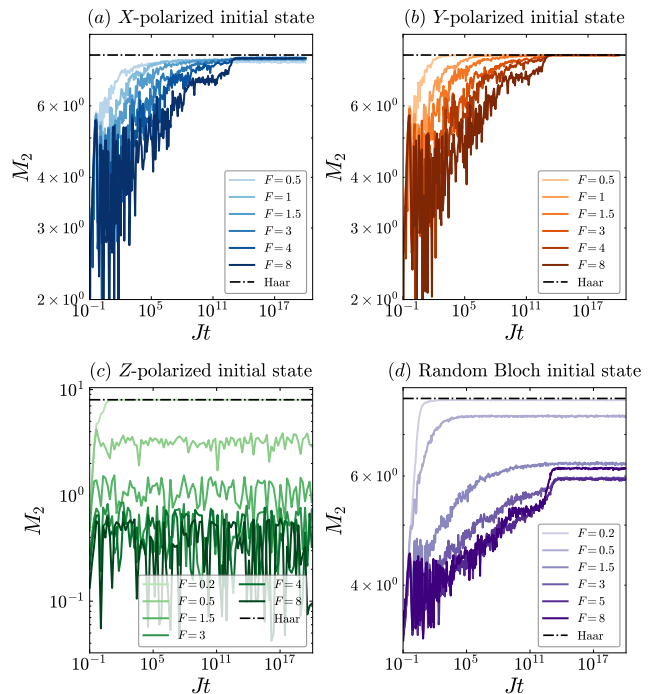


Figure 1. *Time evolution of the SRE-2.* SRE-2 M_2 as a function of dimensionless time Jt with system size $L = 10$ for four initial states: (a) X -polarized, (b) Y -polarized, (c) Z -polarized, and (d) Bloch sphere random product state. Colored curves correspond to different field strengths F (Cf. legends). The black dash-dotted line indicates the Haar-random saturation value M_2^{Haar} for the corresponding system size $L = 10$.

and quantify the deviation from it by $\Delta M_2 \equiv M_2^{\text{Haar}} - M_2$. All numerical calculations were carried out with the TensorCircuit-NG [136] and Qiskit [137].

A first robust observation is that increasing F systematically slows down the generation of M_2 , and for certain initial states also suppresses the long-time plateau. At fixed size $L = 10$, both the X -polarized and Y -polarized product states exhibit a characteristic structure: a rapid initial rise of $M_2(t)$, followed by a broad slow-growth regime, and eventual saturation at long times; moreover, the approach to the plateau becomes dramatically slower as F increases [Fig. 1(a,b)]. Random Bloch product states display the same qualitative slow-growth-and-saturation pattern [Fig. 1(d)], but with a noticeably stronger sensitivity of the plateau to F : for stronger tilts the saturation value can remain well below M_2^{Haar} , corresponding to a sizable long-time ΔM_2 . In sharp contrast, the Z -polarized initial state stays at very small $M_2(t)$ over the entire time window and shows pronounced temporal fluctuations without a clear monotonic slow-growth trend [Fig. 1(c)], demonstrating strong initial-state selectivity in the production of nonstabilizer resources under the same constrained dynamics. The system-size dependence confirms that the slow growth and saturation observed above are generic for a broad class of initial states. For the X -polarized, Y -polarized, and random Bloch initial states, the time traces for $L = 6, 8, 10, 12, 14$ consistently show slow growth over wide

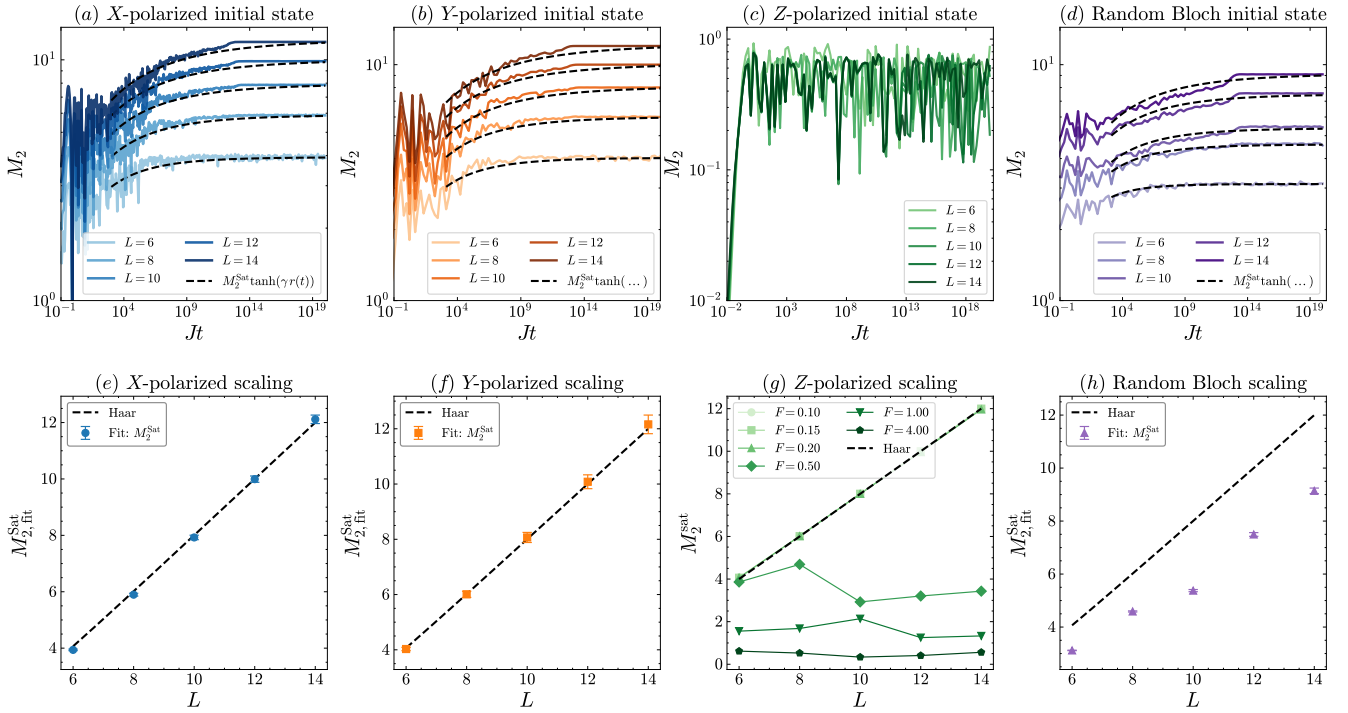


Figure 2. *Dynamics and scaling of the SRE-2*. (a-d) Time evolution of the SRE-2 M_2 versus dimensionless time t for (a) X -polarized, (b) Y -polarized, (c) Z -polarized, and (d) random Bloch product initial states. The colored curves correspond to system sizes $L = 6, 8, 10, 12, 14$, with color intensity increasing from light ($L = 6$) to dark ($L = 14$). Black dashed curves in (a, b, d) indicate fits to the logarithmic growth model Eq. (8). (e, f, h) Scaling of the fitted saturation values $M_{2,\text{fit}}^{\text{Sat}}$ versus system size L for the (e) X -polarized, (f) Y -polarized, and (h) random Bloch initial states. The black dashed line represents the theoretical Haar value $M_2^{\text{Haar}} \approx L - 2$. (g) Saturation magic M_2^{Sat} versus L for varying field strengths F . The data shows a crossover from volume-law like scaling at small F to area-law behavior at large F .

time windows followed by saturation, with the plateau increasing with L [Fig. 2(a,b,d)]. We fit these curves using the growth form introduced in the analytical part (black dashed lines in Fig. 2(a,b,d)), obtaining stable estimates of the saturation values used in the scaling analysis below. By comparison, the Z -polarized state remains dominated by low-valued, strongly fluctuating $M_2(t)$ across all studied sizes [Fig. 2(c)], motivating a separate emphasis on its saturation scaling versus F .

The extracted long-time plateaus reveal distinct finite-size scaling behaviors across initial-state families. For the X - and Y -polarized initial states, the fitted saturation values $M_{2,\text{fit}}^{\text{Sat}}$ grow approximately linearly with L and closely track the Haar reference (black dashed line) over the accessible sizes [Fig. 2(e,f)], indicating near-Haar, volume-law like nonstabilizerness at long times. For random Bloch product states, the saturation values also increase with L , but remain systematically below the Haar benchmark [Fig. 2(h)], consistent with a persistent “non-Haar” deviation in the long-time regime. The Z -polarized case shows a particularly strong F -dependence: at small F the saturation values increase with L and approach the Haar line, while at larger F the L -dependence is strongly suppressed and the plateau tends toward a much smaller, weakly size-dependent value [Fig. 2(g)], i.e., a crossover from volume-law like behavior to area-law like scaling as the tilt is increased.

We next characterize the ETH-SMBL crossover using long-time observables. The deviation ΔM_2 increases sharply with F and shows consistent crossing behavior across system sizes $L = 8, 10, 12, 14$ [Fig. 3(a)]; the inset demonstrates a finite-size collapse with $F_c \approx 0.19$ and $\nu \approx 0.53$. As an entanglement-based counterpart, the half-chain entanglement entropy $S_{L/2}$ decreases markedly as F is increased [Fig. 3(b)], and its inset shows an analogous collapse with $F_c \approx 0.23$ and $\nu \approx 0.46$. Taken together, these collapses suggest a consistent crossover from a more ETH-like regime to a constrained SMBL-like regime, while highlighting that ΔM_2 and $S_{L/2}$ provide complementary perspectives on the same dynamical crossover.

Finally, we examine the relationship between nonstabilizerness and entanglement through parametric plots of the time evolution in the $(S_{L/2}, M_2)$ plane. For the Y -polarized initial state at fixed $L = 10$, the trajectories for different SMBL tilts largely fall onto a single-valued curve, which is well described by Eq. (8) [Fig. 3(c)]. For random Bloch product states, the raw trajectories show systematic offsets as F is varied; however, after rescaling $M_2 \rightarrow M_2/f(F)$ with an L -independent factor $f(F)$, the data collapse improves and the common relation is again captured by Eq. (8) [Fig. 3(d)]. This indicates that in the SMBL regime the growth of entanglement and the generation of nonstabilizerness remain tightly correlated, while the quantitative mapping can be modified by initial-state struc-

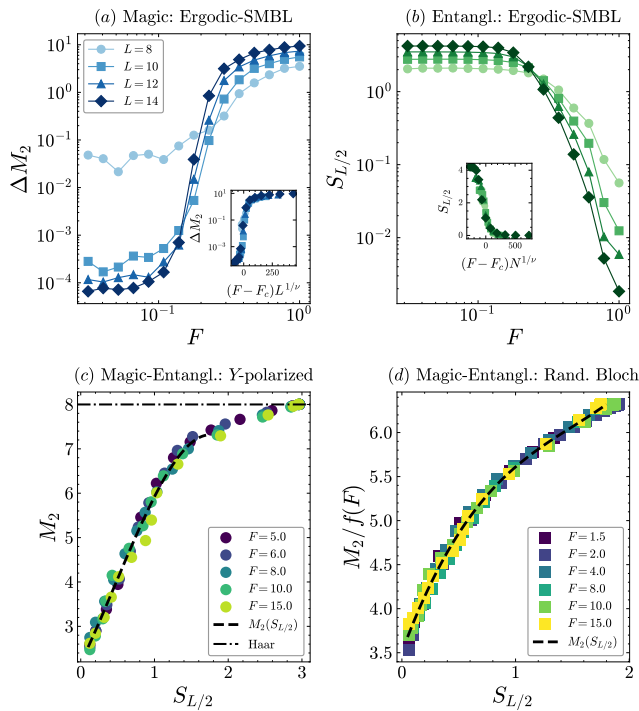


Figure 3. *ETH-SMBL crossover in magic and entanglement.* (a) ΔM_2 versus field strength F for system sizes $L=8, 10, 12, 14$. Inset: finite-size collapse of ΔM_2 versus $(F-F_c)L^{1/\nu}$ with $F_c \approx 0.19$ and $\nu \approx 0.53$. (b) Half-chain entanglement entropy $S_{L/2}$ versus F for the same sizes. Inset: finite-size collapse of $S_{L/2}$ versus $(F-F_c)L^{1/\nu}$ with $F_c \approx 0.23$ and $\nu \approx 0.46$. (c) Parametric relation between SRE M_2 and entanglement $S_{L/2}$ for a Y -polarized initial state at fixed $L=10$ and several SMBL F values with Gaussian-smoothed time traces. The black dashed curve is a polynomial fit $M_2(S_{L/2})$ with Eq. (8), and the dash-dotted line marks the Haar saturation value. (d) Same as (c) for Bloch sphere random product initial states, plotting the rescaled SRE-2 $M_2/f(F)$, where $f(F)$ is L -independent rescaled function; the dashed curve is a fit $M_2(S_{L/2})$.

ture and tilt strength in a way that can be partially absorbed into a simple rescaling.

In a nutshell, we demonstrate that stronger tilts generically slow down the growth of $M_2(t)$ and can reduce its long-time plateau; the saturation scaling is strongly initial-state dependent, with a pronounced volume-to-area-law like crossover for the Z -polarized state at large F ; and the long-time behaviors of ΔM_2 and $S_{L/2}$ jointly support a crossover from ETH-like to SMBL-like dynamics, alongside a clear functional relation between M_2 and $S_{L/2}$ in the SMBL regime.

V. EXPERIMENTAL REALIZATION

We outline an experimentally viable protocol in a linear trapped-ion chain [133, 138, 139] to digitally simulate transverse-field Ising dynamics in the presence of a purely linear Stark tilt and, from a single measurement data set, extract both the half-chain Rényi-2 entanglement entropy and the SRE-2 M_2 . The detailed gate compilation, calibration

procedures, unbiased estimators, and uncertainty analysis are provided Cf. Appendix B.

We consider a chain of L ions encoding L qubits, with computational basis states $|0\rangle, |1\rangle$ defined by state-dependent fluorescence detection. Ion-resolved readout implements a projective measurement in the Z basis, returning a bitstring $s \in \{0, 1\}^L$. Ions are indexed along the chain as $i = 0, 0, \dots, L-1-1$, and this ordering fixes the spatial profile of the linear tilt. The target trapped-ions Hamiltonian is

$$H = \sum_{i<j} J_{ij} Z_i Z_j + h \sum_{i=0}^{L-1} X_i + F \sum_{i=0}^{L-1} i Z_i, \quad (9)$$

where J_{ij} are effective long-range Ising couplings, h is the transverse-field strength, and F is the Stark-gradient parameter. We sample the dynamics at discrete times $t_k = k \delta t$ for integer $k \geq 0$, with digital step size δt .

A calibration stage precedes the dynamical experiment to map experimental controls onto (J_{ij}, h, F) . Operationally, h is set via single-qubit Rabi oscillations that determine the pulse-area-to-rotation-angle conversion, thereby fixing the transverse-field step angle $\theta = 2h \delta t$. The coupling matrix J_{ij} is obtained by enabling the entangling interaction for controlled durations and extracting the resulting two-body phases and/or correlation signals. The linear tilt F is calibrated through ion-resolved Ramsey phase accumulation: the measured Z -frequency shifts scale linearly with the ion index i , and any deviations from strict linearity are recorded as a systematic uncertainty. Implementation-level details and practical diagnostics are discussed in Appendix B.

To implement time evolution, we use a second-order symmetric decomposition. A native long-range two-body interaction is available in trapped ions and, together with global basis rotations, yields an effective ZZ evolution realizing the $\sum_{i<j} J_{ij} Z_i Z_j$ term. The transverse-field contribution is implemented as a global single-qubit rotation $\prod_i R_x^{(i)}(\theta)$. The Stark tilt yields a diagonal evolution equivalent to a product of local Z rotations with ion-dependent phases $\phi_i = 2Fi \delta t$, which can be implemented via ion-resolved AC-Stark shifts or, equivalently, tracked as phase-frame updates. In the circuit description we group the two-body ZZ evolution and the tilt into a single diagonal block U_{diag} , and define one symmetric digital step as

$$U_{\text{step}}(\delta t) = U_{\text{diag}}(\delta t/2) U_X(\delta t) U_{\text{diag}}(\delta t/2), \\ U(t_k) \approx [U_{\text{step}}(\delta t)]^k, \quad (10)$$

with $t_k = k \delta t$. The corresponding gate ordering, timing windows, and error structure are specified in Appendix B.

We probe both structured and typical dynamical regimes by preparing several families of product initial states, including fully Z -polarized, X -polarized $|+\rangle^{\otimes L}$, Y -polarized $|+_y\rangle^{\otimes L}$, and a set of random product states generated by independent single-qubit Bloch-sphere sampling. For the random ensemble, we repeat the full protocol for each sample and report observables averaged over the ensemble to reduce finite-size fluctuations. State-preparation recipes are given in Appendix B.

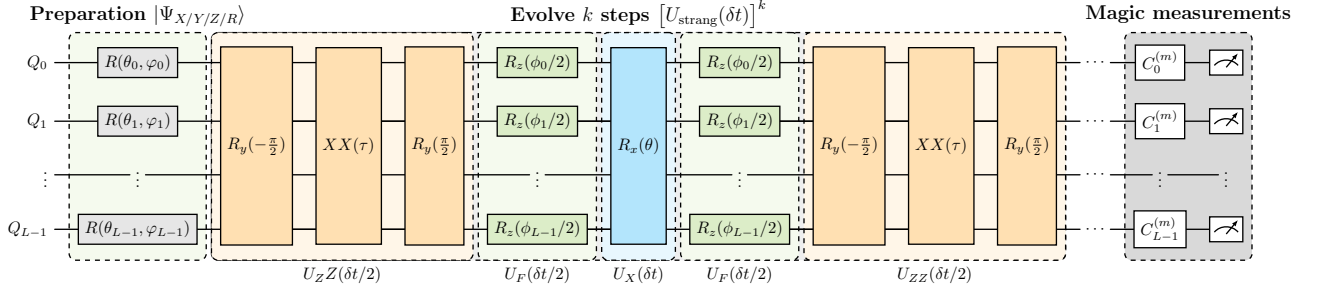


Figure 4. Circuit for digitally simulating the tilted transverse-field Ising model using a second-order Strang step repeated k times, followed by local single-qubit Clifford randomized measurements to extract $S_2(A, t)$ and $M_2(t)$ from the same bitstring data.

At each time point t_k , we extract both entanglement and nonstabilizerness using a local randomized measurement protocol based on single-qubit Clifford operations followed by computational-basis readout. Concretely, we sample N_U local Clifford settings

$$C^{(m)} = \bigotimes_{i=0}^{L-1} c_i^{(m)}, \quad (11)$$

with $c_i^{(m)} \in \mathcal{C}_1$ and $m = 1, \dots, N_U$, apply $C^{(m)}$ to the evolved state $\rho(t_k)$, and measure all qubits in the Z basis N_M times to obtain bitstrings $\{s_\alpha^{(m)}\}_{\alpha=1}^{N_M}$.

The half-chain Rényi-2 entanglement entropy is defined as $S_2(A, t) = -\log_2 \text{Tr}[\rho_A(t)^2]$ with $\rho_A(t) = \text{Tr}_{A^c} \rho(t)$, where $A = \{0, 0, \dots, L - 1/2 - 1\}$ is the left half of the chain. Using the same bitstring data, we estimate the subsystem purity $\text{Tr}[\rho_A^2]$ via collision statistics built from Hamming-weight kernels, and then set $S_2(A, t_k) = -\log_2 P_A(t_k)$. From the same data we also estimate the global purity $\text{Tr}[\rho(t_k)^2]$, which serves both as a decoherence diagnostic and as a mixedness correction for the magic estimator. The explicit unbiased estimators are given in Appendix B.

More importantly, to quantify nonstabilizerness SRE-2, defined through the Pauli fourth moment. Let \mathcal{P}_L denote the L -qubit Pauli operators up to phase. Define $W(t_k) = D^{-2} \sum_{P \in \mathcal{P}_L} \langle P \rangle_{t_k}^4$, where $\langle P \rangle_{t_k} = \text{Tr}[P \rho(t_k)]$ and use the mixed-state-consistent form

$$M_2(t_k) = -\log_2 \left[\frac{D W(t_k)}{\text{Tr}(\rho(t_k)^2)} \right], \quad (12)$$

which reduces to $M_2 \simeq -\log_2[D W]$ when $\rho(t_k)$ remains close to pure. In practice, $W(t_k)$ is estimated from the same randomized-measurement data via a four-bitstring Hamming-weight kernel, requiring $N_M \geq 4$, and combined with the estimated global purity to correct for experimental mixedness. The explicit estimator and kernel are given in Appendix B. The total number of single-shot measurements per time point is $N_{\text{tot}} = N_U \times N_M$. Increasing N_U primarily suppresses fluctuations due to finite random-unitary sampling, while increasing N_M primarily reduces within-setting shot noise; we enforce $N_M \geq 4$ for the fourth-moment estimator. We quantify statistical uncertainties via bootstrap resampling over the

Clifford-setting index m , which preserves estimator structure while providing robust error bars. The pictorial representation pervious description of the architecture is shown in Fig. 4.

VI. CONCLUSION AND OUTLOOK

In this work we investigated the generation and scaling of nonstabilizerness in a clean setting exhibiting Stark many-body localization. We considered a tilted transverse-field Ising chain and quantified complexity using the stabilizer Rényi entropy M_2 , in parallel with standard entanglement diagnostics. We find that, deep in the strong-tilt SMBL regime where transport is strongly suppressed and the dynamics are constrained, $M_2(t)$ still exhibits a robust slow growth over extended time windows before saturating to a finite-size plateau. This shows that SMBL is not Clifford-trivial: even when the dynamics are constrained, the system can still generate genuine non-Clifford computational resources. Moreover, from long-time observables and finite-size analysis we observe a clear crossover/transition from an ETH-like regime to an SMBL-like regime, and we uncover a tight correlation between magic and entanglement growth in the localized regime with a pronounced dependence on the initial state. On the analytical side, in the strong-tilt limit we derived an effective diagonal description based on a Schrieffer-Wolff approach, where long-range diagonal couplings are factorially suppressed along the Wannier-Stark ladder. This naturally explains the slow advance of the dephasing front and the resulting slow growth of $M_2(t)$. On the experimental side, we proposed a feasible trapped-ion digital-simulation protocol, in which both the Rényi-2 entanglement and M_2 can be extracted from the same local randomized-measurement data, including a practical correction for mixedness. Our work identifies nonstabilizerness as a key probe for constrained localization and disorder-free ergodicity breaking.

Looking forward, it would be intriguing to investigate the interplay between nonstabilizerness dynamics and the quantum Mpemba effect [85, 104, 140–145] in ergodicity-breaking and monitored systems [146–152]. Notably, these studies can be directly implemented on digital quantum processors [153–159], which have already demonstrated significant potential in

simulating quantum many-body phenomena.

ACKNOWLEDGMENTS

J.-X. Zhong was supported by the National Natural Science Foundation of China (Grant Nos. 12374046 and 11874316), the Shanghai Science and Technology Innovation Action Plan

(Grant No. 24LZ1400800), the National Basic Research Program of China (Grant No. 2015CB921103), and the Program for Changjiang Scholars and Innovative Research Teams in Universities (Grant No. IRT13093). H.-Z. Li is supported by a China Scholarship Council Scholarship.

-
- [1] R. P. Feynman, Simulating physics with computers, *International Journal of Theoretical Physics* **21**, 467 (1982).
- [2] S. Lloyd, Universal quantum simulators, *Science* **273**, 1073 (1996).
- [3] P. W. Shor, Polynomial-time algorithms for prime factorization and discrete logarithms on a quantum computer, *SIAM Journal on Computing* **26**, 1484 (1997).
- [4] L. K. Grover, Quantum mechanics helps in searching for a needle in a haystack, *Physical Review Letters* **79**, 325 (1997).
- [5] E. Bernstein and U. Vazirani, Quantum complexity theory, *SIAM Journal on Computing* **26**, 1411 (1997).
- [6] S. Aaronson and A. Arkhipov, The computational complexity of linear optics, in *Proceedings of the 43rd ACM Symposium on Theory of Computing (STOC)* (2011) pp. 333–342.
- [7] H.-S. Zhong *et al.*, Quantum computational advantage using photons, *Science* **370**, 1460 (2020).
- [8] W. Kretschmer, S. Grewal, M. DeCross, J. A. Gerber, K. Gilmore, D. Gresh, N. Hunter-Jones, K. Mayer, B. Neyenhuis, D. Hayes, and S. Aaronson, Demonstrating an unconditional separation between quantum and classical information resources, [arXiv:2509.07255](https://arxiv.org/abs/2509.07255) (2025).
- [9] D. Gottesman, The heisenberg representation of quantum computers, [arXiv:quant-ph/9807006](https://arxiv.org/abs/quant-ph/9807006) (1998).
- [10] S. Aaronson and D. Gottesman, Improved simulation of stabilizer circuits, *Phys. Rev. A* **70**, 052328 (2004).
- [11] E. Chitambar and G. Gour, Quantum resource theories, *Rev. Mod. Phys.* **91**, 025001 (2019).
- [12] Z.-W. Liu and A. Winter, Many-body quantum magic, *PRX Quantum* **3**, 020333 (2022).
- [13] L. Leone, S. F. Oliviero, and A. Hamma, Stabilizer Rényi Entropy, *Physical Review Letters* **128**, 050402 (2022).
- [14] L. Leone and L. Bittel, Stabilizer entropies are monotones for magic-state resource theory, *Phys. Rev. A* **110**, L040403 (2024).
- [15] E. Tirrito, P. S. Tarabunga, G. Lami, T. Chanda, L. Leone, S. F. E. Oliviero, M. Dalmonte, M. Collura, and A. Hamma, Quantifying nonstabilizerness through entanglement spectrum flatness, *Phys. Rev. A* **109**, L040401 (2024).
- [16] X. Turkeshi, M. Schirò, and P. Sierant, Measuring nonstabilizerness via multifractal flatness, *Physical Review A* **108**, 042408 (2023).
- [17] X. Turkeshi, A. Dymarsky, and P. Sierant, Pauli spectrum and nonstabilizerness of typical quantum many-body states, *Phys. Rev. B* **111**, 054301 (2025).
- [18] X. Turkeshi, E. Tirrito, and P. Sierant, Magic spreading in random quantum circuits, *Nat. Commun.* **16**, 2575 (2025).
- [19] B. Jasser, J. Odavić, and A. Hamma, Stabilizer entropy and entanglement complexity in the sachdev-ye-kitaev model, [arXiv:2502.03093](https://arxiv.org/abs/2502.03093) (2025).
- [20] M. Viscardi, M. Dalmonte, A. Hamma, and E. Tirrito, Interplay of entanglement structures and stabilizer entropy in spin models, [arXiv:2503.08620](https://arxiv.org/abs/2503.08620) (2025).
- [21] D. Iannotti, G. Esposito, L. Campos Venuti, and A. Hamma, Entanglement and Stabilizer entropies of random bipartite pure quantum states, *Quantum* **9**, 1797 (2025).
- [22] S. Cusumano, L. C. Venuti, S. Cepollaro, G. Esposito, D. Iannotti, B. Jasser, J. O. c, M. Viscardi, and A. Hamma, Non-stabilizerness and violations of chsh inequalities, [arXiv:2504.03351](https://arxiv.org/abs/2504.03351) (2025).
- [23] L. Bittel and L. Leone, Operational interpretation of the stabilizer entropy, [arXiv:2507.22883](https://arxiv.org/abs/2507.22883) (2025).
- [24] N. D. Varikuti, S. Bandyopadhyay, and P. Hauke, Impact of clifford operations on non-stabilizing power and quantum chaos, [arXiv:2505.14793](https://arxiv.org/abs/2505.14793) (2025).
- [25] E. Tirrito, X. Turkeshi, and P. Sierant, Anticoncentration and nonstabilizerness spreading under ergodic quantum dynamics, [arXiv:2412.10229](https://arxiv.org/abs/2412.10229) (2025).
- [26] P. Zhang, S. Zhou, and N. Sun, Stabilizer rényi entropy and its transition in the coupled sachdev-ye-kitaev model, [arXiv:2509.17417](https://arxiv.org/abs/2509.17417) (2025).
- [27] D. Qian and J. Wang, Quantum nonlocal nonstabilizerness, *Phys. Rev. A* **111**, 052443 (2025).
- [28] C. P. Moca, D. Sticlet, B. Dóra, A. Valli, D. Szombathy, and G. Zaránd, Non-stabilizerness generation in a multi-particle quantum walk, [arXiv:2504.19750](https://arxiv.org/abs/2504.19750) (2025).
- [29] N. Dowling, P. Kos, and X. Turkeshi, Magic resources of the heisenberg picture, *Phys. Rev. Lett.* **135**, 050401 (2025).
- [30] S. Bera and M. Schirò, Non-stabilizerness of sachdev-ye-kitaev model, [arXiv:2502.01582](https://arxiv.org/abs/2502.01582) (2025).
- [31] S. Masot-Llima and A. Garcia-Saez, Stabilizer tensor networks: Universal quantum simulator on a basis of stabilizer states, *Phys. Rev. Lett.* **133**, 230601 (2024).
- [32] S. Aditya, A. Summer, P. Sierant, and X. Turkeshi, Mpemba effects in quantum complexity, [arXiv:2509.22176](https://arxiv.org/abs/2509.22176) (2025).
- [33] T. Hernández-Yanes, P. Sierant, J. Zakrzewski, and M. Płodzień, Non-stabilizerness in quantum-enhanced metrological protocols, [arXiv:2510.01380](https://arxiv.org/abs/2510.01380) (2025).
- [34] P. R. N. Falcão, P. Sierant, J. Zakrzewski, and E. Tirrito, Magic dynamics in many-body localized systems, [arXiv:2503.07468](https://arxiv.org/abs/2503.07468) (2025).
- [35] D. Sticlet, B. Dóra, D. Szombathy, G. Zaránd, and C. P. Moca, Non-stabilizerness in open XXZ spin chains: Universal scaling and dynamics, [arXiv:2504.11139](https://arxiv.org/abs/2504.11139) (2025).
- [36] E. Tirrito, P. S. Tarabunga, D. S. Bhakuni, M. Dalmonte, P. Sierant, and X. Turkeshi, Universal spreading of nonstabilizerness and quantum transport, [arXiv:2506.12133](https://arxiv.org/abs/2506.12133) (2025).
- [37] Y. Zhang and Y. Gu, Quantum magic dynamics in random circuits, [arXiv:2410.21128](https://arxiv.org/abs/2410.21128) (2024).
- [38] C. Cao, G. Cheng, A. Hamma, L. Leone, W. Munizzi, and S. F. E. Oliviero, Gravitational back-reaction is magical, [arXiv:2403.07056](https://arxiv.org/abs/2403.07056) (2025).
- [39] P. S. Tarabunga and C. Castelnovo, Magic in generalized

- roksar-kivelson wavefunctions, [Quantum](#) **8**, 1347 (2024).
- [40] X. Qian, J. Huang, and M. Qin, Augmenting a finite-temperature tensor network with clifford circuits, [Phys. Rev. B](#) **112**, 115150 (2025).
- [41] X. Qian, J. Huang, and M. Qin, Clifford circuits augmented time-dependent variational principle, [Phys. Rev. Lett.](#) **134**, 150404 (2025).
- [42] J. Huang, X. Qian, and M. Qin, Nonstabilizerness entanglement entropy: A measure of hardness in the classical simulation of quantum many-body systems with tensor network states, [Phys. Rev. A](#) **112**, 012425 (2025).
- [43] X. Qian, J. Huang, and M. Qin, Augmenting density matrix renormalization group with clifford circuits, [Phys. Rev. Lett.](#) **133**, 190402 (2024).
- [44] M. Frau, P. S. Tarabunga, M. Collura, E. Tirrito, and M. Dalmonte, Stabilizer disentangling of conformal field theories, [SciPost Phys.](#) **18**, 165 (2025).
- [45] C. Fan, X. Qian, H.-C. Zhang, R.-Z. Huang, M. Qin, and T. Xiang, Disentangling critical quantum spin chains with clifford circuits, [Phys. Rev. B](#) **111**, 085121 (2025).
- [46] J. Huang, X. Qian, and M. Qin, Clifford circuits augmented matrix product states for fermion systems, [arXiv:2501.00413](#) (2024).
- [47] Y.-M. Ding, Z. Wang, and Z. Yan, Evaluating many-body stabilizer rényi entropy by sampling reduced pauli strings: Singularities, volume law, and nonlocal magic, [PRX Quantum](#) **6**, 030328 (2025).
- [48] D. A. Korbany, M. J. Gullans, and L. Piroli, Long-range nonstabilizerness and phases of matter, [arXiv:2502.19504](#) (2025).
- [49] P. S. Tarabunga and T. Haug, Efficient mutual magic and magic capacity with matrix product states, [arXiv:2504.07230](#) (2025).
- [50] D. Szombathy, A. Valli, C. P. Moca, L. Farkas, and G. Zaránd, Independent stabilizer rényi entropy and entanglement fluctuations in random unitary circuits, [arXiv:2501.11489](#) (2025).
- [51] Z.-Y. Hou, C. Cao, and Z.-C. Yang, Stabilizer entanglement enhances magic injection, [arXiv:2503.20873](#) (2025).
- [52] M. Hoshino, M. Oshikawa, and Y. Ashida, Stabilizer rényi entropy and conformal field theory, [arXiv:2503.13599](#) (2025).
- [53] P. S. Tarabunga and E. Tirrito, Magic transition in measurement-only circuits, [arXiv:2407.15939](#) (2024).
- [54] E. Tirrito, L. Lumia, A. Paviglianiti, G. Lami, A. Silva, X. Turkishi, and M. Collura, Magic phase transitions in monitored gaussian fermions, [arXiv:2507.07179](#) (2025).
- [55] C. Wang, Z.-C. Yang, T. Zhou, and X. Chen, Magic transition in monitored free fermion dynamics, [arXiv:2507.10688](#) (2025).
- [56] G. C. Santra, A. Windey, S. Bandyopadhyay, A. Legramandi, and P. Hauke, Complexity transitions in chaotic quantum systems, [arXiv:2505.09707](#) (2025).
- [57] T. Haug, L. Aolita, and M. Kim, Probing quantum complexity via universal saturation of stabilizer entropies, [Quantum](#) **9**, 1801 (2025).
- [58] T. Haug and L. Piroli, Stabilizer entropies and nonstabilizerness monotones, [Quantum](#) **7**, 1092 (2023).
- [59] T. Haug and L. Piroli, Quantifying nonstabilizerness of matrix product states, [Physical Review B](#) **107**, 035148 (2023).
- [60] G. Lami and M. Collura, Nonstabilizerness via Perfect Pauli Sampling of Matrix Product States, [Phys. Rev. Lett.](#) **131**, 180401 (2023).
- [61] G. Lami and M. Collura, Unveiling the Stabilizer Group of a Matrix Product State, [Phys. Rev. Lett.](#) **133**, 010602 (2024).
- [62] P. S. Tarabunga, E. Tirrito, T. Chanda, and M. Dalmonte, Many-body magic via pauli-markov chains—from criticality to gauge theories, [PRX Quantum](#) **4**, 040317 (2023).
- [63] P. S. Tarabunga, E. Tirrito, M. C. Bañuls, and M. Dalmonte, Nonstabilizerness via matrix product states in the pauli basis, [Phys. Rev. Lett.](#) **133**, 010601 (2024).
- [64] J. Preskill, Quantum computing in the NISQ era and beyond, [Quantum](#) **2**, 79 (2018).
- [65] L. Daguerre, R. Blume-Kohout, N. C. Brown, D. Hayes, and I. H. Kim, Experimental demonstration of high-fidelity logical magic states from code switching, [Phys. Rev. X](#) **15**, 041008 (2025).
- [66] D. Aasen, M. Aghaee, Z. Alam, M. Andrzejczuk, A. Antipov, M. Astafev, L. Avilovas, A. Barzegar, B. Bauer, J. Becker, J. M. Bello-Rivas, U. Bhaskar, A. Bocharov, S. Boddapati, D. Bohn, *et al.*, Roadmap to fault tolerant quantum computation using topological qubit arrays, [arXiv:2502.12252](#) (2025).
- [67] T. Peham, L. Schmid, L. Berent, M. Müller, and R. Wille, Automated synthesis of fault-tolerant state preparation circuits for quantum error-correction codes, [PRX Quantum](#) **6**, 020330 (2025).
- [68] A. I. Larkin and Y. N. Ovchinnikov, Quasiclassical method in the theory of superconductivity, [Soviet Physics JETP](#) **28**, 1200 (1969).
- [69] S. H. Shenker and D. Stanford, Black holes and the butterfly effect, [Journal of High Energy Physics](#) **2014**, 067 (2014).
- [70] J. Maldacena, S. H. Shenker, and D. Stanford, A bound on chaos, [Journal of High Energy Physics](#) **2016**, 106 (2016).
- [71] B. Swingle, Unscrambling the physics of out-of-time-order correlators, [Nature Physics](#) **14**, 988 (2018).
- [72] K. Hashimoto, K. Murata, and R. Yoshii, Out-of-time-order correlators in quantum mechanics, [Journal of High Energy Physics](#) **2017**, 138 (2017).
- [73] D. A. Roberts and B. Yoshida, Chaos and complexity by design, [Journal of High Energy Physics](#) **2017**, 121 (2017).
- [74] J. Cotler, N. Hunter-Jones, J. Liu, and B. Yoshida, Chaos, complexity, and random matrices, [Journal of High Energy Physics](#) **2017**, 048 (2017).
- [75] L. Leone, S. F. E. Oliviero, Y. Zhou, and A. Hamma, Quantum chaos is quantum, [Quantum](#) **5**, 453 (2021).
- [76] K. Goto, T. Nosaka, and M. Nozaki, Probing chaos by magic monotones, [Physical Review D](#) **106**, 126009 (2022).
- [77] A. Paviglianiti, G. Lami, M. Collura, and A. Silva, Estimating nonstabilizerness dynamics without simulating it, [PRX Quantum](#) **6**, 030320 (2025).
- [78] T. Prosen, Many-body quantum chaos and dual-unitarity round-a-face, [Chaos](#) **31**, 093101 (2021).
- [79] K. Huang, X. Li, D. A. Huse, and A. Chan, Out-of-time-order correlations and quantum chaos, [Scholarpedia](#) **18**, 55237 (2023).
- [80] P. Hayden and J. Preskill, Black holes as mirrors: quantum information in random subsystems, [Journal of High Energy Physics](#) **2007**, 120 (2007).
- [81] Y. Sekino and L. Susskind, Fast scramblers, [Journal of High Energy Physics](#) **2008**, 065 (2008).
- [82] P. Hosur, X.-L. Qi, D. A. Roberts, and B. Yoshida, Chaos in quantum channels, [Journal of High Energy Physics](#) **2016**, 004 (2016).
- [83] C. W. von Keyserlingk, T. Rakovszky, F. Pollmann, and S. L. Sondhi, Operator hydrodynamics, OTOCs, and entanglement growth in systems without conservation laws, [Physical Review X](#) **8**, 021013 (2018).
- [84] V. Khemani, A. Vishwanath, and D. A. Huse, Operator spreading and the emergence of dissipative hydrodynamics under unitary evolution with conservation laws, [Physical Review X](#) **8**, 031057 (2018).

- [85] S. Liu, H.-K. Zhang, S. Yin, and S.-X. Zhang, Symmetry restoration and quantum mpemba effect in symmetric random circuits, *Physical Review Letters* **133**, 140405 (2024).
- [86] S. Liu, H.-K. Zhang, S. Yin, S.-X. Zhang, and H. Yao, Symmetry restoration and quantum mpemba effect in many-body localization systems, *Science Bulletin* **70**, 3991–3996 (2025).
- [87] H. Yu, Z.-X. Li, and S.-X. Zhang, Symmetry breaking dynamics in quantum many-body systems, *Chinese Physics Letters* **42**, 110602 (2025).
- [88] C. Liu and W. W. Ho, Solvable entanglement dynamics in quantum circuits with generalized space-time duality, *Phys. Rev. Res.* **7**, L012011 (2025).
- [89] C. Dankert, R. Cleve, J. Emerson, and E. Livine, Exact and approximate unitary 2-designs and their application to fidelity estimation, *Phys. Rev. A* **80**, 012304 (2009).
- [90] C. Dankert, R. Cleve, J. Emerson, and E. Livine, Exact and approximate unitary 2-designs and their application to fidelity estimation, *Physical Review A* **80**, 012304 (2009).
- [91] A. W. Harrow and R. A. Low, Random quantum circuits are approximate 2-designs, *Communications in Mathematical Physics* **291**, 257 (2009).
- [92] F. G. S. L. Brandão, A. W. Harrow, and M. Horodecki, Local random quantum circuits are approximate polynomial-designs, *Communications in Mathematical Physics* **346**, 397 (2016).
- [93] W. W. Ho and S. Choi, Exact emergent quantum state designs from quantum chaotic dynamics, *Physical Review Letters* **128**, 060601 (2022).
- [94] M. Ippoliti and W. W. Ho, Dynamical purification and the emergence of quantum state designs from the projected ensemble, *PRX Quantum* **4**, 030322 (2023).
- [95] P. W. Claeys and A. Lamacraft, Quantum many-body scars and space-time crystalline order from magnon condensation, *Phys. Rev. Lett.* **129**, 100601 (2022).
- [96] P. W. Claeys, A. Lamacraft, and J. Vicary, From dual-unitary to biunitary: a 2-categorical model for exactly-solvable many-body quantum dynamics, *Journal of Physics A: Mathematical and Theoretical* **57**, 335301 (2024).
- [97] Z. Cheng, E. Huang, V. Khemani, M. J. Gullans, and M. Ippoliti, Emergent unitary designs for encoded qubits from coherent errors and syndrome measurements, *PRX Quantum* **6**, 030333 (2025).
- [98] D. A. Abanin, E. Altman, I. Bloch, and M. Serbyn, Colloquium: Many-body localization, thermalization, and entanglement, *Reviews of Modern Physics* **91**, 021001 (2019).
- [99] R. Nandkishore and D. A. Huse, Many-body localization and thermalization in quantum statistical mechanics, *Annual Review of Condensed Matter Physics* **6**, 15 (2015).
- [100] F. Alet and N. Laflorencie, Many-body localization: An introduction and selected topics, *Comptes Rendus Physique* **19**, 498 (2018).
- [101] S.-X. Zhang and H. Yao, Universal properties of many-body localization transitions in quasiperiodic systems, *Phys. Rev. Lett.* **121**, 206601 (2018).
- [102] S. Liu, S.-X. Zhang, C.-Y. Hsieh, S. Zhang, and H. Yao, Discrete time crystal enabled by stark many-body localization, *Phys. Rev. Lett.* **130**, 120403 (2023).
- [103] S. Liu, S.-X. Zhang, C.-Y. Hsieh, S. Zhang, and H. Yao, Probing many-body localization by excited-state variational quantum eigensolver, *Phys. Rev. B* **107**, 024204 (2023).
- [104] S. Liu, H.-K. Zhang, S. Yin, S.-X. Zhang, and H. Yao, Symmetry restoration and quantum mpemba effect in many-body localization systems, *Science Bulletin* **70**, 3991 (2025).
- [105] H.-Z. Li, X.-J. Yu, and J.-X. Zhong, Non-hermitian stark many-body localization, *Phys. Rev. A* **108**, 043301 (2023).
- [106] W. Wang, H.-Z. Li, and J.-X. Zhong, Non-hermitian many-body localization in asymmetric chains with long-range interaction, [arXiv:2510.08277](https://arxiv.org/abs/2510.08277) (2025).
- [107] P. Sala, T. Rakovszky, R. Verresen, M. Knap, and F. Pollmann, Ergodicity-breaking arising from hilbert space fragmentation in dipole-conserving hamiltonians, *Physical Review X* **10**, 011047 (2020).
- [108] V. Khemani, M. Hermele, and R. M. Nandkishore, Localization from hilbert space shattering: from theory to physical realizations, *Physical Review B* **101**, 174204 (2020).
- [109] S. Scherg, T. Kohlert, P. Sala, F. Pollmann, H. M. Bharath, I. Bloch, and M. Aidelsburger, Observing non-ergodicity due to kinetic constraints in tilted fermi-hubbard chains, *Nature Communications* **12**, 4490 (2021).
- [110] M. Brenes, M. Dalmonte, M. Heyl, and A. Scardicchio, Many-body localization dynamics from gauge invariance, *Physical Review Letters* **120**, 030601 (2018).
- [111] P. Karpov, R. Verdel, Y.-P. Huang, M. Schmitt, and M. Heyl, Disorder-free localization in an interacting two-dimensional lattice gauge theory, *Physical Review Letters* **126**, 130401 (2021).
- [112] M. Schulz, C. A. Hooley, R. Moessner, and F. Pollmann, Stark many-body localization, *Physical Review Letters* **122**, 040606 (2019).
- [113] M. Glück, A. R. Kolovsky, and H. J. Korsch, Wannier–stark resonances in optical and semiconductor superlattices, *Physics Reports* **366**, 103 (2002).
- [114] S. Nandy, J. Herbrych, Z. Lenarčič, A. Głodkowski, P. Prelovšek, and M. Mierzejewski, Emergent dipole moment conservation and subdiffusion in tilted chains, *Physical Review B* **109**, 115120 (2024).
- [115] H.-Z. Li, M. Wan, and J.-X. Zhong, Fate of non-hermitian free fermions with wannier-stark ladder, *Phys. Rev. B* **110**, 094310 (2024).
- [116] Y.-J. Zhao, H.-Z. Li, X. Huang, S.-Z. Li, and J.-X. Zhong, Fate of pseudomobility edges and multiple states in a non-hermitian wannier-stark lattice, *Phys. Rev. B* **111**, 014315 (2025).
- [117] X. Huang, H.-Z. Li, Y.-J. Zhao, S. Liu, and J.-X. Zhong, Quantum feedback induced entanglement relaxation and dynamical phase transition in monitored free fermion chains with a wannier-stark ladder, *Phys. Rev. B* **111**, 184302 (2025).
- [118] Y.-J. Zhao, X. Huang, Y.-R. Zhang, H.-Z. Li, and J.-X. Zhong, Entanglement phases and phase transitions in monitored free fermion system due to localizations, [arXiv:2509.09538](https://arxiv.org/abs/2509.09538) (2025).
- [119] S. Moudgalya, B. A. Bernevig, and N. Regnault, Quantum many-body scars and hilbert space fragmentation: a review of exact results, *Reports on Progress in Physics* **85**, 086501 (2022).
- [120] D. Adler, D. Wei, M. Will, K. Srakaew, S. Agrawal, P. Weckesser, R. Moessner, F. Pollmann, I. Bloch, and J. Zeiher, Observation of hilbert space fragmentation and fractonic excitations in 2d, *Nature* **636**, 80 (2024).
- [121] A. Nahum, S. Vijay, and J. Haah, Operator spreading in random unitary circuits, *Phys. Rev. X* **8**, 021014 (2018).
- [122] J. Odavić, M. Viscardi, and A. Hamma, Stabilizer entropy in nonintegrable quantum evolutions, *Phys. Rev. B* **112**, 104301 (2025).
- [123] M. Serbyn, Z. Papić, and D. A. Abanin, Local conservation laws and the structure of the many-body localized states, *Phys. Rev. Lett.* **111**, 127201 (2013).
- [124] P. R. N. Falcão, P. Sierant, J. Zakrzewski, and E. Tirrito,

- Nonstabilizerness dynamics in many-body localized systems, *Phys. Rev. Lett.* **135**, 240404 (2025).
- [125] C. Cao, Y. Zhou, S. Tannu, N. Shannon, and R. Joynt, Exploiting many-body localization for scalable variational quantum simulation, *Quantum* **9**, 1942 (2025).
- [126] K. Agarwal, E. Altman, E. Demler, S. Gopalakrishnan, D. A. Huse, and M. Knap, Rare-region effects and dynamics near the many-body localization transition, *Annalen der Physik* **529**, 1600326 (2017).
- [127] W. De Roeck and F. m. c. Huveneers, Stability and instability towards delocalization in many-body localization systems, *Phys. Rev. B* **95**, 155129 (2017).
- [128] T. Thiery, F. m. c. Huveneers, M. Müller, and W. De Roeck, Many-body delocalization as a quantum avalanche, *Phys. Rev. Lett.* **121**, 140601 (2018).
- [129] P. Sala, T. Rakovszky, R. Verresen, M. Knap, and F. Pollmann, Ergodicity breaking arising from hilbert space fragmentation in dipole-conserving hamiltonians, *Phys. Rev. X* **10**, 011047 (2020).
- [130] E. van Nieuwenburg, Y. Baum, and G. Refael, From bloch oscillations to many-body localization in clean interacting systems, *Proceedings of the National Academy of Sciences* **116**, 9269 (2019).
- [131] L. Amico, R. Fazio, A. Osterloh, and V. Vedral, Entanglement in many-body systems, *Rev. Mod. Phys.* **80**, 517 (2008).
- [132] R. Horodecki, P. Horodecki, M. Horodecki, and K. Horodecki, Quantum entanglement, *Rev. Mod. Phys.* **81**, 865 (2009).
- [133] S. F. E. Oliviero, L. Leone, A. Hama, and S. Lloyd, Measuring magic on a quantum processor, *npj Quantum Information* **8**, 148 (2022).
- [134] T. Haug and M. Kim, Scalable measures of magic resource for quantum computers, *PRX Quantum* **4**, 010301 (2023).
- [135] P. Niroula, C. D. White, Q. Wang, S. Johri, D. Zhu, C. Monroe, C. Noel, and M. J. Gullans, Phase transition in magic with random quantum circuits, *Nature Physics* **20**, 1786–1792 (2024).
- [136] S.-X. Zhang, J. Allcock, Z.-Q. Wan, S. Liu, J. Sun, H. Yu, X.-H. Yang, J. Qiu, Z. Ye, Y.-Q. Chen, C.-K. Lee, Y.-C. Zheng, S.-K. Jian, H. Yao, C.-Y. Hsieh, and S. Zhang, Tensorcircuit: a quantum software framework for the nisq era, *Quantum* **7**, 912 (2023).
- [137] A. Javadi-Abhari, M. Treinish, K. Krsulich, C. J. Wood, J. Lishman, J. Gacon, S. Martiel, P. D. Nation, L. S. Bishop, A. W. Cross, B. R. Johnson, and J. M. Gambetta, Quantum computing with qiskit, [arXiv:2405.08810](https://arxiv.org/abs/2405.08810) (2024).
- [138] A. Sørensen and K. Mølmer, Quantum computation with ions in thermal motion, *Phys. Rev. Lett.* **82**, 1971 (1999).
- [139] T. Brydges, A. Elben, P. Jurcevic, B. Vermersch, C. Maier, B. P. Lanyon, P. Zoller, R. Blatt, and C. F. Roos, Probing rényi entanglement entropy via randomized measurements, *Science* **364**, 260–263 (2019).
- [140] F. Ares, P. Calabrese, and S. Murciano, The quantum mpemba effects, *Nature Reviews Physics* **7**, 451–460 (2025).
- [141] X. Turkeshi, P. Calabrese, and A. De Luca, Quantum mpemba effect in random circuits, *Phys. Rev. Lett.* **135**, 040403 (2025).
- [142] H. Yu, S. Liu, and S.-X. Zhang, Quantum mpemba effects from symmetry perspectives, *AAPPS Bulletin* **35**, 17 (2025).
- [143] A. Summer, M. Moroder, L. P. Bettmann, X. Turkeshi, I. Marvian, and J. Goold, A resource theoretical unification of mpemba effects: classical and quantum, [arXiv:2507.16976](https://arxiv.org/abs/2507.16976) (2025).
- [144] S. Aditya, A. Summer, P. Sierant, and X. Turkeshi, Mpemba effects in quantum complexity, [arXiv:2509.22176](https://arxiv.org/abs/2509.22176) (2025).
- [145] G. Di Giulio, X. Turkeshi, and S. Murciano, Measurement-induced symmetry restoration and quantum mpemba effect, *Entropy* **27**, 407 (2025).
- [146] B. Skinner, J. Ruhman, and A. Nahum, Measurement-induced phase transitions in the dynamics of entanglement, *Phys. Rev. X* **9**, 031009 (2019).
- [147] Y. Li, X. Chen, and M. P. A. Fisher, Measurement-driven entanglement transition in hybrid quantum circuits, *Phys. Rev. B* **100**, 134306 (2019).
- [148] S. Liu, M.-R. Li, S.-X. Zhang, S.-K. Jian, and H. Yao, Universal kardar-parisi-zhang scaling in noisy hybrid quantum circuits, *Phys. Rev. B* **107**, L201113 (2023).
- [149] S. Liu, M.-R. Li, S.-X. Zhang, and S.-K. Jian, Entanglement structure and information protection in noisy hybrid quantum circuits, *Phys. Rev. Lett.* **132**, 240402 (2024).
- [150] S. Liu, M.-R. Li, S.-X. Zhang, S.-K. Jian, and H. Yao, Noise-induced phase transitions in hybrid quantum circuits, *Phys. Rev. B* **110**, 064323 (2024).
- [151] X.-J. Yu, S. Yang, S. Liu, H.-Q. Lin, and S.-K. Jian, Gapless symmetry-protected topological states in measurement-only circuits, [arXiv:2501.03851](https://arxiv.org/abs/2501.03851) (2025).
- [152] W. Wang, S. Liu, J. Li, S.-X. Zhang, and S. Yin, Relaxation critical dynamics in measurement-induced phase transitions, [arXiv:2502.13408](https://arxiv.org/abs/2502.13408) (2025).
- [153] J. M. Koh, T. Tai, Y. H. Phee, W. E. Ng, and C. H. Lee, Stabilizing multiple topological fermions on a quantum computer, *npj Quantum Information* **8**, 16 (2022).
- [154] J. M. Koh, T. Tai, and C. H. Lee, Realization of higher-order topological lattices on a quantum computer, *Nature Communications* **15**, 5807 (2024).
- [155] T. Chen, R. Shen, C. H. Lee, and B. Yang, High-fidelity realization of the AKLT state on a NISQ-era quantum processor, *SciPost Phys.* **15**, 170 (2023).
- [156] R. Shen, T. Chen, B. Yang, Y. Zhong, and C. H. Lee, Robust simulations of many-body symmetry-protected topological phase transitions on a quantum processor, [arXiv:2503.08776](https://arxiv.org/abs/2503.08776) (2025).
- [157] S. Miyashita, T. Satoh, M. Sugawara, N. Benchasattabuse, K. M. Nakanishi, M. Hajdušek, H. Choi, and R. V. Meter, Digital quantum simulator for the time-dependent dirac equation using discrete-time quantum walks, [arXiv:2305.19568](https://arxiv.org/abs/2305.19568) (2023).
- [158] N. K. Mohan, R. Bhowmick, D. Kumar, and R. Chaurasiya, Digital quantum simulations of hong-ou-mandel interference, [arXiv:2402.17522](https://arxiv.org/abs/2402.17522) (2024).
- [159] B. Fauseweh, Quantum many-body simulations on digital quantum computers: State-of-the-art and future challenges, *Nat. Commun.* **15**, 2123 (2024).

Appendix A: Analysis for the nonstabilizerness dynamics of SML

In this section, we elaborate the analysis in the main text. Consider Eq. (1),

$$H = H_0 + V; \quad H_0 = \sum_{j=1}^L (F j Z_j + J Z_j Z_{j+1}); \quad V = h \sum_{j=1}^L X_j, \quad (\text{A1})$$

in the strong-tilt regime $F \gg J, h$. We construct a Schrieffer-Wolff (SW) effective Hamiltonian $H_{\text{eff}} = e^S H e^{-S}$ with an anti-Hermitian generator $S^\dagger = -S$. Using the Baker-Campbell-Hausdorff identity $e^S A e^{-S} = A + [S, A] + \frac{1}{2}[S, [S, A]] + \dots$ and the expansion $S = S^{(1)} + O(\hbar^2)$ with $S^{(1)} = O(\hbar)$, truncation to $O(\hbar^2)$ yields

$$H_{\text{eff}} = H_0 + V + [S^{(1)}, H_0] + \frac{1}{2}[S^{(1)}, V] + O(\hbar^3). \quad (\text{A2})$$

The SW condition removes the leading off-diagonal term (in the eigenbasis of H_0),

$$[H_0, S^{(1)}] = V. \quad (\text{A3})$$

Define the diagonal operator $\Delta_j \equiv Fj + J(Z_{j-1} + Z_{j+1})$. Using $[Z_j, Y_j] = 2iX_j$, one finds $[H_0, Y_j] = -2i\Delta_j X_j$, hence an explicit choice is $S^{(1)} = \sum_j \frac{i\hbar}{2} \Delta_j^{-1} Y_j$. Substituting back gives the standard second-order form

$$\begin{aligned} H_{\text{eff}} &= H_0 + \frac{1}{2}[S^{(1)}, V] + O(\hbar^3) \\ &= H_0 + \sum_j \frac{\hbar^2}{2} \Delta_j^{-1} Z_j + O(\hbar^3). \end{aligned} \quad (\text{A4})$$

The long-time dephasing dynamics is controlled by higher-order diagonal multi-spin terms generated by the SW procedure. To define distance- r diagonal couplings, take the Z -product eigenbasis $\{|s\rangle\}$ and the diagonal part $H_{\text{eff}}^{(d)} \equiv \sum_s |s\rangle \langle s| H_{\text{eff}} |s\rangle \langle s|$. Introduce the subset operators $Z_S \equiv \prod_{i \in S} Z_i$ for $S \subseteq \{0, \dots, L-1\}$. Since $\{Z_S\}$ forms an orthogonal basis of diagonal operators, one has the unique expansion

$$H_{\text{eff}}^{(d)} = \sum_{S \subseteq \{0, \dots, L-1\}} c_S Z_S, \quad c_S = 2^{-L} \text{Tr}(H_{\text{eff}}^{(d)} Z_S). \quad (\text{A5})$$

Define the two-body diagonal coefficients $\tilde{J}_{ij} \equiv c_{\{i,j\}}$ and the distance- r coupling scale by the spatial root-mean-square

$$J_{\text{eff}}(r) \equiv \left(\frac{1}{L-r} \sum_{i=1}^{L-r} \tilde{J}_{i,i+r}^2 \right)^{1/2}. \quad (\text{A6})$$

In the strong-tilt regime, a diagonal coupling spanning distance r is generated by a shortest chain of virtual processes whose denominators are dominated by the Stark ladder. A scaling estimate gives a numerator $(\hbar)^r$, while intermediate-state detunings accumulate linearly, $E_i - E_{k_m} \sim mF$ for $m=1, \dots, r-1$, producing $\prod_{m=1}^{r-1} (E_i - E_{k_m}) \sim F^{r-1} (r-1)!$. Absorbing path-counting and $O(J/F)$ corrections into a non-universal prefactor J_0 with $J_0 \sim \hbar$, one obtains the factorially suppressed form

$$J_{\text{eff}}(r) \sim J_0 \frac{(\hbar/F)^{r-1}}{(r-1)!}. \quad (\text{A7})$$

Define the dephasing front $r(t)$ by the phase-accumulation condition $t J_{\text{eff}}(r(t)) \sim 1$. Writing $n \equiv r-1$ and using Stirling $\ln n! \simeq n \ln n - n$, one finds $t J_0 \frac{(\hbar/F)^n}{n!} \sim 1$, then

$$n \ln \left(\frac{n}{e \hbar/F} \right) \simeq \ln(t J_0). \quad (\text{A8})$$

Solving with the principal branch W_0 of the Lambert function defined by $W_0(x) e^{W_0(x)} = x$ gives the closed form

$$r(t) \simeq 1 + \frac{\ln(t J_0)}{W_0 \left(\frac{\ln(t J_0)}{e \hbar/F} \right)}. \quad (\text{A9})$$

For the SRE-2 $M_2(t)$, the dephasing-dominated regime is captured by an extensive growth with the active length scale $r(t)$ and saturation to a finite-size plateau M_{sat} . A compact single-parameter closure that is linear at small argument and saturating at long times is

$$M_2(t) \simeq M_{\text{sat}} \tanh(\gamma r(t)), \quad (\text{A10})$$

where γ is a growth coefficient and $J_0 \sim h$ sets the microscopic time scale.

Appendix B: Experimental accessibility

We propose an experimental protocol on a linear trapped-ion chain to digitally simulate the transverse-field Ising dynamics in the presence of a purely linear Stark tilt, and to measure, as functions of time, both the half-chain Rényi-2 entanglement entropy and SRE at $k=2$ from a common data set. The platform encodes L qubits in L ions, with each qubit represented by two long-lived internal states $|0\rangle$ and $|1\rangle$. The computational basis $\{|0\rangle, |1\rangle\}$ is fixed by state-dependent fluorescence detection: one of the two levels is coupled to a closed cycling transition and yields bright fluorescence under resonant illumination, whereas the other level remains dark, such that ion-resolved photon counts implement a projective measurement in the Z basis and return a bitstring $s \in \{0, 1\}^L$. The ions are indexed along the chain as $i=0, 0, \dots, L-1-1$, and this ordering defines the spatial profile of the linear tilt.

The target Hamiltonian we aim to implement is

$$H = \sum_{i<j} J_{ij} Z_i Z_j + h \sum_{i=0}^{L-1} X_i + F \sum_{i=0}^{L-1} i Z_i, \quad (\text{B1})$$

where J_{ij} denotes the effective long-range Ising couplings, h is the transverse-field strength, and F is the gradient that generates the linear Stark tilt. We propose to sample the dynamics at discrete times $t_k = k \delta t$, where δt is a digital time step and k is a nonnegative integer. A calibration stage is included to establish the mapping from experimental controls to the model parameters. In particular, the transverse-field amplitude can be calibrated via single-qubit Rabi oscillations, which determine the pulse-area-to-angle conversion and thereby fix the implementation of $\theta = 2h \delta t$. The coupling matrix J_{ij} can be calibrated by enabling the global entangling interaction for controlled durations and extracting accumulated two-body phases or correlation signals; if appropriate, a compact parametrization may be obtained by fitting to a power-law form. The tilt gradient F can be calibrated by ion-resolved Ramsey phase accumulation, since the extracted Z frequency shifts scale linearly with the ion index i ; any deviation from strict linearity can be recorded as a systematic uncertainty.

We propose to implement the time evolution using a digital simulation based on a second-order Strang splitting. In a standard trapped-ion implementation, a long-range XX interaction is naturally available via a Mølmer-Sørensen mechanism [138],

$$U_{XX}(\tau) = \exp\left[-i\tau \sum_{i<j} J_{ij} X_i X_j\right]. \quad (\text{B2})$$

A global basis change maps the native interaction to an effective ZZ interaction,

$$U_{ZZ}(\tau) = \left[\prod_{i=0}^{L-1} R_y^{(i)}\left(\frac{\pi}{2}\right) \right] U_{XX}(\tau) \left[\prod_{i=0}^{L-1} R_y^{(i)}\left(-\frac{\pi}{2}\right) \right]. \quad (\text{B3})$$

The transverse-field step is realized as

$$U_X(\delta t) = \prod_{i=0}^{L-1} R_x^{(i)}(\theta), \quad (\text{B4})$$

where $\theta = 2h \delta t$. The linear Stark tilt generates a diagonal evolution over one time step,

$$U_F(\delta t) = \exp\left[-i\delta t F \sum_{i=0}^{L-1} i Z_i\right] = \prod_{i=0}^{L-1} R_z^{(i)}(\phi_i), \quad (\text{B5})$$

here $\phi_i = 2Fi \delta t$ and $\prod_i R_z^{(i)}(\phi_i)$ may be implemented by ion-resolved detunings or AC-Stark shifts that accumulate phases, or equivalently by phase-frame updates that account for the same unitary action in the circuit description via the angles ϕ_i .

We propose to combine the two-body ZZ term and the linear tilt into a single diagonal block, and define the Strang step as

$$U_{\text{Strang}}(\delta t) = U_{\text{diag}}\left(\frac{\delta t}{2}\right) U_X(\delta t) U_{\text{diag}}\left(\frac{\delta t}{2}\right), \quad (\text{B6})$$

$$U_{\text{diag}}\left(\frac{\delta t}{2}\right) = U_{ZZ}\left(\frac{\delta t}{2}\right) \prod_{i=0}^{L-1} R_z^{(i)}\left(\frac{\phi_i}{2}\right). \quad (\text{B7})$$

The evolution to time t_k is then implemented as

$$U(t_k) \approx \left[U_{\text{Strang}}(\delta t) \right]^k, \quad (\text{B8})$$

with $t_k = k \delta t$. At the gate level, one Strang step consists of an interaction half-step realizing $U_{ZZ}(\delta t/2)$ through a global R_y basis change surrounding a global entangling window $U_{XX}(\delta t/2)$, together with a linear-phase half-step $\prod_i R_z^{(i)}(\phi_i/2)$, followed by the transverse-field step $\prod_i R_x^{(i)}(\theta)$, and finally the same linear-phase half-step and interaction half-step applied in reverse order to enforce the Strang symmetry.

We propose to prepare four families of product initial states in the main text in order to probe both structured and typical dynamics. The pictorial representation of the architecture is shown in Fig. 4. The Z -polarized state is $|\Psi_Z\rangle$. The X -polarized state is $|\Psi_X\rangle = |+\rangle^{\otimes L}$ with $|+\rangle = \frac{1}{\sqrt{2}}(|0\rangle + |1\rangle)$, prepared by a global $R_y(\pi/2)$ rotation on $|0\rangle^{\otimes L}$. The Y -polarized state is $|\Psi_Y\rangle = |+_y\rangle^{\otimes L}$ with $|+_y\rangle = \frac{1}{\sqrt{2}}(|0\rangle + i|1\rangle)$, prepared by a global $R_x(-\pi/2)$ rotation. Finally, we propose a fully random Bloch-sphere ensemble implemented as a set $\{|\Psi_{\text{rnd}}^{(r)}\rangle\}_{r=1}^{N_{\text{rnd}}}$ of Haar-uniform random product states, where each ion independently samples $\varphi \in [0, 2\pi)$ uniformly and samples $\cos \theta$ uniformly in $[-1, 1]$, and is prepared via $R_z(\varphi)R_y(\theta)|0\rangle$ to realize $|\psi(\theta, \varphi)\rangle = \cos \frac{\theta}{2} |0\rangle + e^{i\varphi} \sin \frac{\theta}{2} |1\rangle$. In the random-initial-state case, we propose to repeat the full protocol for each sample index r and report observables averaged over r to suppress finite-size fluctuations and access typical behavior.

To extract both the half-chain Rényi-2 entanglement entropy and the M_2 dynamics from a common data set, inspired by Ref. [133], we propose a local randomized measurement protocol that requires only single-qubit Clifford operations followed by computational-basis readout. For each time point t_k , we sample N_U local single-qubit Clifford unitaries

$$C^{(m)} = \bigotimes_{i=0}^{L-1} c_i^{(m)}, \quad (\text{B9})$$

with $c_i^{(m)} \in \mathcal{C}_1$ and $m = 1, 2, \dots, N_U$ apply $C^{(m)}$ to the evolved state $\rho(t_k)$, and then measure all qubits in the computational basis N_M times. This yields bitstrings $s_\alpha^{(m)} \in \{0, 1\}^L$ with $\alpha = 1, 2, \dots, N_M$. For the half-chain analysis, we denote by $s_{\alpha, A}^{(m)}$ the restriction of $s_\alpha^{(m)}$ to the subsystem $A = \{0, 0, \dots, L - 1/2 - 1\}$. Conceptually, each $C^{(m)}$ maps computational-basis readout to a random local Pauli measurement basis, and the local single-qubit Clifford ensemble provides the unitary-design property needed to reconstruct the relevant second- and fourth-order moments from collision statistics of the measured bitstrings.

The half-chain Rényi-2 entanglement entropy is defined as $S_2(A, t) = -\log_2 \text{Tr}[\rho_A(t)^2]$, where $\rho_A(t) = \text{Tr}_{A^c} \rho(t)$ and A is the left half of the chain. We propose to estimate the subsystem purity $P_A(t_k) = \text{Tr}[\rho_A(t_k)^2]$ from the same bitstrings using the kernel

$$K_2(u, v) = (-2)^{-\text{wt}(u \oplus v)}, \quad (\text{B10})$$

where \oplus denotes bitwise Exclusive OR (XOR) and $\text{wt}(\bullet)$ is the Hamming weight. The estimator takes the U-statistic form

$$P_A(t_k) = \frac{1}{N_U} \sum_{m=1}^{N_U} \frac{1}{N_M(N_M - 1)} \sum_{\alpha \neq \beta} (-2)^{-\text{wt}(s_{\alpha, A}^{(m)} \oplus s_{\beta, A}^{(m)})}, \quad (\text{B11})$$

where $S_2(A, t_k) = -\log_2 P_A(t_k)$. In parallel, we propose to estimate the global purity $P(t_k) = \text{Tr}[\rho(t_k)^2]$ from the same data which is useful both as a diagnostic of decoherence and as an explicit mixedness correction for M_2 via

$$P(t_k) = \frac{1}{N_U} \sum_{m=1}^{N_U} \frac{1}{N_M(N_M - 1)} \sum_{\alpha \neq \beta} (-2)^{-\text{wt}(s_\alpha^{(m)} \oplus s_\beta^{(m)})}. \quad (\text{B12})$$

To quantify nonstabilizerness, we propose to use SRE at $k = 2$ defined through the Pauli fourth moment. Let $D = 2^L$ and let \mathcal{P}_L denote L -qubit Pauli operators up to an overall phase. Define

$$W(t_k) := D^{-2} \sum_{P \in \mathcal{P}_L} \langle P \rangle_{t_k}^4, \quad \langle P \rangle_{t_k} = \text{Tr}[P \rho(t_k)]. \quad (\text{B13})$$

A mixed-state-consistent definition of the M_2 is then

$$M_2(t_k) = -\log_2 \left[\frac{D W(t_k)}{\text{Tr}(\rho(t_k)^2)} \right], \quad (\text{B14})$$

which reduces to $M_2(t_k) \approx -\log_2[D W(t_k)]$ when $\rho(t_k)$ remains close to pure. We propose to estimate $W(t_k)$ using the four-string kernel

$$K_4(u_1, u_2, u_3, u_4) = (-2)^{-\text{wt}(u_1 \oplus u_2 \oplus u_3 \oplus u_4)}, \quad (\text{B15})$$

and the unbiased U-statistic estimator (requiring $N_M \geq 4$)

$$\begin{aligned} & \mathcal{W}(t_k) \\ &= \frac{1}{N_U} \sum_{m=1}^{N_U} \frac{1}{\binom{N_M}{4}} \sum_{\alpha < \beta < \gamma < \delta} (-2)^{-\text{wt}(s_\alpha^{(m)} \oplus s_\beta^{(m)} \oplus s_\gamma^{(m)} \oplus s_\delta^{(m)})}. \end{aligned} \quad (\text{B16})$$

Combining $\mathcal{W}(t_k)$ with the experimentally accessible global purity estimate $\mathcal{P}(t_k)$, we propose the following experimental estimator for the M_2 :

$$\mathcal{M}_2(t_k) = -\log_2 \left[\frac{D \mathcal{W}(t_k)}{P(t_k)} \right]. \quad (\text{B17})$$

In the near-pure regime where $\mathcal{P}(t_k) \simeq 1$, this expression simplifies to $\mathcal{M}_2(t_k) \simeq -\log_2[D \mathcal{W}(t_k)]$, while in regimes with appreciable decoherence it provides a direct mixedness correction via the ratio form. Repeating the same protocol for all t_k yields time traces $S_2(A, t)$ and $M_2(t)$ that can be compared on equal footing to elucidate the interplay between entanglement growth and nonstabilizerness generation under transverse-field Ising dynamics with a linear Stark tilt. We propose to quantify statistical uncertainties by bootstrap resampling over the local Clifford setting index m , which separates initial-state sampling fluctuations from finite-shot measurement noise while preserving the estimator structure. The total number of single-shot measurements per time point is $N_{\text{tot}} = N_U \times N_M$. In resource allocation, increasing N_U primarily suppresses fluctuations due to finite unitary sampling, whereas increasing N_M primarily suppresses within-setting shot noise; we propose to choose (N_U, N_M) by balancing these contributions under an overall measurement-budget constraint, with the additional practical requirement $N_M \geq 4$ for the fourth-order estimator $\mathcal{W}(t_k)$.